This is a repository copy of *Suitability of the Southern Australia Integrated Marine Observing System's (SA-IMOS) HF-Radar for operational forecasting*.

White Rose Research Online URL for this paper:
https://eprints.whiterose.ac.uk/140753/

Version: Accepted Version

Article:

James, C., Collopy, M., Wyatt, L.R. orcid.org/0000-0002-9483-0018 et al. (1 more author) (2019) Suitability of the Southern Australia Integrated Marine Observing System's (SA-IMOS) HF-Radar for operational forecasting. Journal of Operational Oceanography, 12 (2). pp. 73-85. ISSN 1755-876X

https://doi.org/10.1080/1755876X.2019.1567450

This is an Accepted Manuscript of an article published by Taylor & Francis in Journal of Operational Oceanography on 24/01/2019, available online: http://www.tandfonline.com/10.1080/1755876X.2019.1567450

Reuse
Items deposited in White Rose Research Online are protected by copyright, with all rights reserved unless indicated otherwise. They may be downloaded and/or printed for private study, or other acts as permitted by national copyright laws. The publisher or other rights holders may allow further reproduction and re-use of the full text version. This is indicated by the licence information on the White Rose Research Online record for the item.

Takedown
If you consider content in White Rose Research Online to be in breach of UK law, please notify us by emailing eprints@whiterose.ac.uk including the URL of the record and the reason for the withdrawal request.

eprints@whiterose.ac.uk
https://eprints.whiterose.ac.uk/

Acknowledgments

HF-Radar data was sourced from the Integrated Marine Observing System (IMOS) - IMOS is a national collaborative research infrastructure, supported by the Australian Government. The Cape du Couedic Waverider Buoy data was supplied by the Australian Bureau of Meteorology. The ADCP wave data was supplied by the SARDI Innovative Solutions 2 (IS2) project. The grid for the wave model was the SAROM grid from the eSA-Marine forecasting system run by SARDI and the Australian Bureau of Meteorology.

Abstract

The IMOS HF-Radar array in South Australia provides observations of the ocean waters south of Spencer Gulf. In addition to ocean surface currents, the data from this array can be processed to provide near-real time observations of wave statistics and wind direction. The Australian Bureau of Meteorology requires access to these observations for forecast modelling but currently only have a single Waverider buoy operating in South Australian waters at Cape du Couedic, south of Kangaroo Island, which provides no directional information. The HF-Radar array could potentially be used to augment the current operational observation systems used by the Bureau. In this paper we evaluate the performance of the HF-Radar system against observations from the Waverider buoy and an automatic weather station at Neptune Island and also compare the HF-Radar observations to a wave model based on the eSA-Marine forecast grid. The results suggest that upgrading the HF-Radar to provide near-real time wave and wind data would provide a new, independent source of environmental observations for the Bureau.

Keywords

HF-Radar, Remote Sensing, South Australia, Waves, Wind direction.

Introduction

Australian Bureau of Meteorology marine forecast products provide detailed text and graphical outputs for a range of different ocean scales from Metro Waters (typically within 5nm offshore), Coastal Zone (out to 60nm around Australia's coastline) to High Seas (south to 50^{O}S). Bureau marine service guidelines mandate the provision of wind wave (sea) and swell components, as well as total significant wave heights to the public. Bureau user surveys consistently acknowledge the value of wave and swell forecast parameters, and highlight the associated safety issues for the marine community.

The Bureau operates a range of ocean observing systems, aiming to inform forecasting centres and the marine community of safety critical components such as wind and wave conditions. The Bureau's ability to verify the accuracy of model and forecast output is critical to real-time operational forecasts and the on-going development of the service. Longstanding wave observing systems such as Waverider buoys are considered crucial to providing the quality marine forecasts and warnings which the Bureau has the responsibility for under the international SOLAS (1974) agreement.

The wave climate in the Southern Ocean is poorly covered by direct observations. Historically most of the information about the wave climate is derived from satellite altimetry or from numerical wave models (Hemer *et al*., 2010). On the South Australian shelf the only continuous observations from the Australian Bureau of Meteorology are from a Waverider buoy moored off Cape du Couedic. These observations are limited to wave heights and period with no directional information.

Ocean based observing systems such as the Cape du Couedic Waverider buoy are often cited as the base for verification of model and forecast outputs, and as such are acknowledged as critical equipment but they are also difficult and expensive to deploy and maintain. Sites such as Cape du Couedic (4nm southwest of the western tip of Kangaroo Island) provide a single point in the wave climate, and whilst such sites are chosen carefully they do not provide data beyond the given location, depth and distance from shore.

The Integrated Marine Observing System's (IMOS) Australian Coastal Ocean Radar Network (ACORN) facility has installed a phased array high frequency radar system around the mouth of Spencer Gulf in South Australia (Figure 1). This array is known as the South Australian Gulfs (SAG) HF array, a Wellen Radar (WERA) phased array system (Gurgel *et al*., 1999) with arrays at Cape Wiles and Cape Spencer. Phased array HF radars receive backscatter from a wide area of the ocean that is resolved into individual cells of area a few square km. The intrinsic spatial resolution of the radar is set in azimuth by the number of antennas in the receive array and the beam-forming method used and in range by the swept bandwidth of the radar. Normally data are either processed or interpolated onto a rectangular grid for ease of display and handling. All these processes mean that the measurements are correlated between neighbouring and, in some cases due to sidelobes, distant cells and any real variability on the scale of a few cells will either be smoothed or lead to unwanted peaks in the radar Doppler spectrum that can be a source of error in the metocean measurements made. Interference and other non-sea signals, e.g. ships, can also lead to errors. One goal of the measurement process is to identify and remove these sources of error either at the signal processing stage or by quality control at the post processing stage.

The main role of HF-Radar is to measure the radial surface currents, which is done by measuring the Doppler shifted power spectrum of the received signals. This is the information used to provide near real-time updates of currents to the IMOS data portal (IMOS, 2017, Cosoli *et al.*, 2018). However, phased array systems like the SAG WERA system can also provide information on a variety of other physical properties including wave information and wind direction (Wyatt *et al*., 2006; Heron and Prytz, 2002). The ACORN facility has recently begun processing the SAG data and producing high quality wave and wind time series. The sources of error mentioned above are more significant when measuring waves since these use more of the radar spectrum and signal-to-noise is also lower.

Previous studies have shown that the wave parameters and wind directions, remotely measured by HF-Radar, show strong correlations with in-situ measurements and wave models (Wyatt *et al*., 1999;

Wyatt *et al*., 2003; Long *et al*., 2011; Hisaki, 2012; Lorente *et al*., 2018). In the case of Spencer Gulf installation the area of coverage encompasses a changing wave climate from near the edge of the continental shelf, through the complex bathymetry between Kangaroo Island and Eyre Peninsula and into the southern part of Spencer Gulf. Data from this type of ocean wave observing system has the potential to provide significant advantages in terms of validation of wave model and forecast output over an area which in this case is critical to the wave energy entering Spencer Gulf and Gulf St Vincent, both of which are high use marine zones. Comparison of existing HF-Radar data with high resolution Bureau models would provide important validation of this operationally utilised model output, not only for South Australia but for near-shore areas around the Australian coast. Future real-time data from HF-Radar systems can enhance forecaster understanding of the complex wave environment and potentially lead to improved forecast and warning products. With adequate quality control, observations from the HF-Radar may prove valuable in future wave model data assimilation schemes (Waters *et al*., 2013).

To this end we have chosen, in this paper, to investigate the potential of HF-Radar to provide high quality wave and wind observations for use, either as validation or assimilated data, in operational forecasting systems. To test HF-Radar performance against observations we will look at two key HF-Radar time series, significant wave height and wind direction, which are derived from different parts of the HF-Radar Doppler spectrum. Significant wave heights are based on measurements of the second order part of the spectrum while wind directions are based on measurements of the first order part of the spectrum. Significant wave height has been found to provide an excellent combination of data quality and availability (Gomez *et al*., 2015) and can be compared against the nearby Cape du Couedic non-directional Waverider buoy while the wind direction can be compared to the winds recorded at the Automated Weather Station (AWS) located on Neptune Island near the area where the HF-Radar observations are made. A wave model of the region is also used for comparison with wave direction observations, for which there are no available in-situ observations, and coupled to a current model to examine spatial differences in wave characteristics.

Performance or skill of the HF-Radar system, are typically assessed against model and in-situ observations using basic statistical metrics – mean, standard deviation, correlation, root-mean-square error (RMSE), and bias (Lorente *et al*., 2018; Long *et al*., 2011; Gomez *et al*., 2015). To this suite of metrics we have added normalized RMSE (NRMSE), calculated by dividing the RMSE by either the mean of the HF-Radar observations or 360^{O} for circular observations, and spectral coherence, over periods ranging from 1 to 12 days, as a measure of the utility of the HF-Radar over typical weather band intervals. The results of all scalar metrics are summarized in Table 1.

Methods

In order to evaluate the performance of the SAG array, a three-way comparison of data between processed HF-Radar output, Australian Bureau of Meteorology observing systems, and a validated wave model of the Southern Australian coastal region was conducted. The validated wave model allows for comparisons including wave directions at the site of the HF-Radar wave measurements which would otherwise be unavailable.

Two sets of observational data were used to test the performance of the wind and wave measurements made by the SAG array. The wave data were from the Waverider Buoy maintained by the Australian Bureau of Meteorology near Cape du Couedic on the south coast of Kangaroo Island and the wind data were from the AWS on Neptune Island just south-west of Spencer Gulf. A separate source of wave observations used to validate the wave model were from an ADCP equipped with a wave package moored near the mouth of Spencer Gulf during the SARDI IS2 project in late 2010 (Middleton *et al*., 2013). The location of the mooring is shown in Figure 1.

The Bureau of Meteorology conducts ocean wave modelling through its investment and development of AUSWAVE (locally developed version of NCEP WAVEWATCH III®, implemented 2010; WMO Guide to Wave Analysis and Forecasting, 1998). Propagation from the open ocean, across the continental shelf, to the critical near-shore zone is derived from pre-computed high resolution (1nm) stationary output from the SWAN near-shore wave model (Booij *et al*., 1999). This experiment also applied the SWAN model, constructed on the main eSA-Marine forecast grid (SAROM, a regional ocean forecasting model run jointly by the Bureau and SARDI: http://pir.sa.gov.au/research/esa_marine) using two non-stationary (time stepping) configurations.

One version was simple wave model forced with swell and surface winds from the ECMWF ERA-Interim product (Dee *et al*., 2011) for the period for which HF-Radar observations were available and a second version was run in a 2-way coupling with the SAROM hydrodynamic model for a short 2 year run (2011-2012) to examine the effects of spatial differences in surface currents at the HF-Radar and Cape du Couedic Site. The coupled ocean model is the Regional Ocean Modelling System (ROMS; https://www.myroms.org/) and was forced on the boundaries by the BRAN global model (Oke, *et al*., 2013), TPOX-8 tidal data (Egbert, *et al*., 2002) and by the ECMWF swell and atmospheric forcing.

The wave model was validated against wave data collected with the Cape du Couedic Waverider buoy (Figure 2, top) and an RDI Workhorse 600Khz ADCP equipped with a wave package within Spencer Gulf (Figure 2, bottom). For the comparison the observational data and model data were both low pass filtered with a 3-hour running average – half the temporal resolution of the ERA-Interim data used to force the model. The model skill is particularly good in the case of the Cape du Couedic site (Table 1) with a strong correlation of r=0.95 (N=5568) and low RMSE of 0.39 m (bias=0.15m). The results for the relatively short time series at Spencer Gulf site were not as strong (Table 1) but still showed good correlation of r=0.8 (N=671) and relatively low RMSE of 0.44m (bias=0.17m). The main limitation on the model performance in Spencer Gulf is the ECMWF atmospheric forcing. While the ECMWF forcing is generally reliable south of KI (which itself is not resolved in the ECMWF interim model), with 6 hourly data and an effective horizontal resolution of approximately 80 km (Dee *et al*., 2011), ECMWF interim forcing lacks the temporal and spatial resolution to provide accurate sea-breeze forcing of the wind waves in Spencer Gulf. Nevertheless, in both cases the root-mean-square error (RMSE) between the modelled output and the observations is less than the 0.5 m precision given for the Bureau's network of Waverider buoys.

The two SAG arrays were originally configured to optimize measurements of ocean currents subject to the geographic constraints of the region. But the locations of the two arrays (Figure 1) also provide a configuration that can measure wave properties. The second order regions in the Doppler spectra are related to the ocean wave directional spectrum via a non-linear integral equation. The Seaview Sensing software, used to generate dual radar wave measurements, uses an iterative integral inversion technique to estimate the directional spectrum, from which wave parameters such as significant wave height, mean wave direction, mean period and peak period can be derived (Wyatt et. al., 2011; Green and Wyatt, 2006, Wyatt et. al., 2009). Inversion is only carried out if the signal to noise at the peak of the second order spectrum is greater than 15dB. At each iteration simulated Doppler spectra using the previous iteration's directional spectrum are compared with the measured spectra and the difference between them is used to either update the directional spectrum for a new iteration or to terminate the process if small enough. The final value of this difference, referred to as the inversion residual, is used to assess the quality of the inversion. Directional spectra and derived parameters are only used if this residual is less than 0.3. Reasons for non-convergence of the scheme (i.e. high values of the residual) are related to low signal to noise away from the second order peak, surface current temporal or spatial variability during the measurement period, interference, ships or low-flying aircraft signals.

Wave data have been processed from three distinct periods. For all sets of data the HF-Radar wave data were generated from the hourly averaged raw Doppler spectra using the Seaview Sensing software and provided on a regular grid. The first period covers approximately 6 months from April 01 till September 21 2011 and were the first HF-Radar data processed with the Seaview software. For this time period only, additional trial thresholding QC procedures were applied, and only the data flagged as good were used. The aim of these procedures was to identify non sea-signals in the

Doppler spectra before inversion but the method is not yet considered robust enough to apply operationally. For this data set the number of rejected data were small. The second period covers over a year and a half from September 25 2013 to May 8 2015 during which a slightly modified grid was used. The third period from May 8 2015 to June 30 2017 covers the period after which the HF-radar operating frequency was increased from 8.512 MHz to 9.330 MHz, otherwise the data were processed in the same manner as the second period.   Only data from the 21 grid cells within 10km of the point with the highest number of QC'd good returns during the first deployment period from all grids were selected.   This point or "hot-spot" lies at -35.54^{O}S, 136.12^{O}E at the approximate centre of the innermost contour of the HF-Radar footprint in Figure 1.   The mean of scalar wave properties and median of wave directions within these cells were then used to generate a time series.   To generate statistical confidence a minimum of N=6 good cells were required to form a median value and a threshold standard deviation of 0.5m was set for significant wave height.

In addition to the wave data it is also possible to estimate the wind direction by applying a wave/wind model to the relative peak amplitudes of the first order Bragg peak components in the Doppler spectra (Wyatt . 2012).   These wind directions assume that the ocean waves responsible for the first order scatter are wind driven and aligned with the wind direction. As was shown in Wyatt *et al*. (2006), this requires that the first order waves are at frequencies higher than the peak of the wind wave spectrum and will fail when wind speeds are low. The wind direction data is included in the HF-Radar data from ACORN for all three periods covered, and is converted to a time series in much the same manner as the wave data, with radar observations for the first period using the circular mean of good observations (N>=6) within the 21 grid cells; the threshold for circular standard deviations in the wind direction was set at 5 degrees.   Because wind directions are calculated from the stronger first-order returns they have a higher signal to noise ratio and provide more high quality observations than the wave data over the same period.

Observations

Waves

The results of the 3-way comparisons of significant wave height and peak wave period between HF-Radar, Waverider Buoy, and model output are presented in Figures 3 and 4 and a 2-way comparison of wave direction between HF-Radar and model output is shown in Figure 5. The model output here is calculated for the position of the HF-Radar footprint rather than the location of the Cape du Couedic Waverider. Significant wave height and peak wave period appear to be in overall agreement between the three estimates, but because the Cape du Couedic Waverider Buoy does not measure directional information, we have to rely on the results of the SWAN model to confirm that the HF-Radar measured wave directions are consistent with the overall pattern of swell propagation in this region. The wave field around South Australia is dominated by swell propagating in from the Southern Ocean out of the south-west (Hemer *et al*., 2010) and both the model and the HF-Radar show this peak swell direction to be from approximately -138^{O} true. The Cape du Couedic/HF-radar comparison extends to June 30 2017.

Wind Direction

The results for wind direction from the three different periods are shown in Figure 6 and compared with the observations from Neptune Island AWS. Again, the model output here is calculated for the position of the HF-Radar but in this case the Neptune Island AWS is within the Radar footprint. The Neptune Island/HF-radar comparison extends to June 30 2017. The AWS wind directions are only reported to within 10 degrees while the HF-Radar derived wind directions are given as single precision floating point values with a much higher degree of precision (<<1 degree).

Results and Analysis

We looked at two forms of comparison to evaluate the HF-Radar performance, temporal correlation of the time series and the coherence spectrum over periods from 1 to 12 days. Because of the consistency of the swell from the Southern Ocean, with significant wave heights rarely dropping below 3m (Figure 3), there was very little significant seasonal variation in the correlations so only results for the full time series are presented here. Correlations, root mean square errors (RMSE), and relative biases were calculated for comparisons between HF-Radar and BoM observations for significant wave height and wind direction; statistics for wind direction were calculated using their circular equivalents for correlation, mean and standard deviation (Fisher, 1993). Because the wind-direction data are likely to be poor when the wind speeds are too low (Wyatt *et al*., 2006), we restricted the wind direction analysis to periods when the AWS indicated that the wind speeds exceeded 5m/s (equivalent to a gentle breeze on the Beaufort scale). Because of the exposed nature of Neptune Island, winds exceed 5m/s more than 88% of the time during the period observations were available. To calculate the coherence between the HF-Radar, with somewhat irregular sampling intervals, and the comparatively continuous in-situ records, the hourly HF-Radar observations were broken down into multiple sequences with only short gaps of 1 day or less. The gaps in these sequences were linearly interpolated over to generate continuous records. The 10-minute Waverider Buoy data was bin averaged to hourly intervals. The Neptune Island AWS data was usually recorded on the hour and half hour (>94% of observations) with 10 degree resolution in wind direction. The remaining directional data was circularly bin averaged into hourly intervals with an effective 5 degree resolution rejecting any observations that did not fall on the hour or half hour. For plotting and coherence calculations the directional data was wrapped to ensure the difference between the two time series did not exceed 180 degrees. The cross-spectrum between the unbroken sequences was computed for as many 256-hour overlapping windows that could be applied without zero padding. The coherence was then calculated with the band-averaged crossspectra from all the unbroken sequences. The 95% confidence interval was estimated using the Monte Carlo method with 100,000 ensembles of white noise for each spectrum computed.

Waves

Despite periodic gaps in the HF-Radar data, visually there is agreement with the Waverider Buoy data in Figures 3 and 4. This is especially significant as the distance between the Waverider Buoy and the centre of the HF-Radar footprint is over 70km and suggests that the spatial coherence scales for waves in this region are reasonably large.

Comparing the significant wave height, the correlation coefficient is 0.90 and RMSE between the two signals is approximately 0.42m (Figure 7, top) which is less than the 0.5m given for the Bureau's Waverider network performance. In comparison, previous studies of radar vs. wave buoy observations show typical correlations for significant wave height of 0.87-0.93 and RMSE 0.36-0.52m for a dual WERA radar system at the Wave Hub site near Cornwall, U.K. (Gomez *et al.*, 2015), correlations of 0.67 and RMSE of 0.48m for a single radar installation in the East China Sea (Hisaki, 2014) and correlations of 0.85-0.91 and RMSE 0.47-0.77m for a 5-CODAR SeaSonde installation along the California Coast (Long *et al.*, 2011).

Differences between measured significant wave heights were typically less than 2m (99.7% of all observations) with a handful of observations (N=20) exceeding 3m. All the outliers occurred during the shorter first period of HF-Radar coverage with the prototype grid and QA/QC procedure described above; the new procedures appear to avoid large outliers. The mean wave height over all periods was 2.9m with a standard deviation of about 1.0m. The total bias over the 10,311 hourly observations is only 6.3cm. The coherence squared spectrum for significant wave height (Figure 7, bottom) shows significant coherence at all periods longer than 1 day with the phase differences indicating a fairly flat response with a near zero mean.

Comparing the peak wave period, the correlation coefficient is 0.80 with an RMSE of 1.3sec (Figure 8, top). In comparison with the previous studies, correlations for peak wave period between 0.53-0.76 and RMSE 1.5-3.2sec were obtained for the dual WERA radar system at the Wave Hub site(Gomez *et al.*, 2015), correlations of 0.59 and RMSE of 1.4sec for mean wave period at the single radar installation in the East China Sea (Hisaki, 2014) and correlations of 0.56-0.61 and RMSE 2.48-3.96sec for the wave period at the California SeaSonde installation (Long *et al.*, 2011).

Comparison of the coupled model output at the site of the HF-Radar footprint and at the site of the Cape du Couedic Buoy indicates that there is a slight weakening of coherence at periods below 2 days (Figure 8, bottom) that is primarily due to the tidal currents in the coupled model and differences in topography. Unfortunately, for reasons discussed above, the ECMWF winds don't allow the model to resolve the wind-driven wave differences which would also be present in the observational data.

Unfortunately the lack of directional information from the Cape du Couedic buoy means an evaluation of the performance of wave direction measurements against observations is not possible. The HF Radar observed swell direction is very steady with a standard deviation in direction of only 17.6^{O} (Table 1), therefore regression and coherence analysis between model and radar are not appropriate measures of radar performance (i.e. correlation is near 0, Table 1), however, the overall bias between the mean directions is only -0.54^{O} indicating that these two estimates of the swell-wave direction are consistent within this region. The agreement between the variations is weak and may also be due to the poor representation of the wind-waves in the model.

Wind

The wind direction shows very strong coherence squared (>0.75) between the HF-Radar and the Neptune Island AWS at all periods with a flat almost negligible phase difference (Figure 10). Unlike the Waverider buoy, the AWS lies well within the HF-Radar footprint (Figure 1) and is only about

25km from the point where the HF-Radar observations are made. Because the wind direction is calculated from the first order part of the Doppler spectrum there are far more hourly observations: 29,734. The circular correlation coefficient is 0.87 and the RMSE in direction is about 26 degrees with an overall bias of -3.6 degrees. Since the wind directions from the AWS are only given to within 10 degrees bins the RMSE is effectively less than 3 bins wide and the bias less than a single bin.

Discussion

The HF-Radar platform provides an alternative source of observations of wind and wave data on the ocean shelf south of Spencer Gulf. Performance of the SAG installation wave observations compare well with other studies (Gomez *et al.*, 2015, Hisaki, 2014, Long *et al.*, 2011), generally showing strong correlations in both time and frequency space. The observations of wind and wave properties also compare well with in-situ measurements by the Neptune Island AWS and the Cape du Couedic Waverider buoy. In particular, the comparisons with wind direction suggest that the HF-Radar could be a useful, higher precision, substitute for the AWS wind directions which also captures the temporal characteristics of the wind direction data across a wide range of periods. The wave data also compares well with observations, particularly at periods longer than 1 day. One advantage that the HF-Radar has over the Cape du Couedic buoy is the ability to measure directional data and directional spectra. In the absence of a proper validation of directional wave data against observations, a numerical model of the wave field during the period of comparison can only confirm that the average HF-Radar directional data is consistent with the simulations.

It is quite possible that the HF-Radar measured wave data is even better than the comparisons with Cape du Couedic suggest. The Waverider buoy is located relatively near the coast of Kangaroo Island (Figure 1) and waves in the area are likely to be influenced by coastal effects including sea-breezes. In contrast, the HF-Radar footprint, where the wave measurements are derived from, is relatively far from any coastal influences. There are also differences in the tidal amplitudes and phases which can modify the local wave-current interactions. A comparison of the coherence squared between the two sites in the coupled model suggests that at the very least, tidal currents do weaken the shorter period coherences (Figure 8). Discrepancies between the two sets of observations can be explained by the different geometry of the two locations and their physical separation – the correlation length scale for swell based on satellite measurements is on the order of 100s of km (Greenslade and Young, 2005).

One of the key questions for evaluating the suitability of the observations for an operational system is the intermittency of the time series. The first point to make is that the wave data depend on analysis of the returns from the second-order regions of the Doppler spectra while the wind data (like the surface current data) are computed from the first-order region. Keeping in mind that the separation of radar sites was optimized for currents rather than waves, this means that there are significantly fewer good data points for the wave data than for the wind data. The second point is that for the present system configuration there are potentially avoidable record gaps due to equipment and power failures that might be alleviated within an operational environment by providing suitable back-up systems. A brief analysis of the wind data coverage from the second and third periods of deployment shows that during the roughly 40,000 hours (4.5 years) data were available in at least one of the 21 cells 88.2% of the time, this drops to 87.7% if we apply our N>=6 criteria for statistical quality. For the wave data over the same period the values are 29.6% and 21.1% respectively. The wave data coverage may not be as bad as those figures suggest however. Most of the intervals (83.8%) are shorter than 3 hours (including data gaps) and if we look at daily averaged, rather than hourly, wave properties the data coverage over the 4.5 years increases to 81.4%.

Conclusion

The performance of the SAG HF Radar as an observational platform for monitoring waves from the southern ocean has been validated against the Cape du Couedic Waverider buoy and is consistent with the performance of a numerical wave model. The SAG HF-Radar has the additional advantage of providing directional information which the current Waverider buoy does not. Differences between the Radar and Waverider observations might be partially explained by differences in tides and coastal geometry at the sites observed.

The HF-radar derived wave statistics and wind directions are well correlated with observed values over a wide range of periods. Performance of this HF-radar installation compares well with other installations with regard to significant wave height and wave period. Data coverage of wind direction, including gaps due to servicing issues, is available at hourly intervals around 88% of the time. Data coverage for the wave data is poorer than the wind direction due to site configuration and processing limitations but can provide daily averaged values around 81% of the time.

The remoteness of the SAG array locations means that it is currently impractical to stream the large amount of data required to do the wave and wind analysis in near-real time. However, recent progress in performing temporal averaging of the raw Doppler spectra at the array sites prior to transmission may be able to address this issue by dramatically reducing the size of the data files being transmitted. In principle, with adequate resourcing, it should be possible to receive the data in a timely manner and allow the SAG HF-Radar to form a part of the Bureau's observation system supplementing the wave information from Cape du Couedic and wind direction observations from the Neptune Island AWS. Future work includes developing a hindcast assimilation scheme for a local wave forecasting model and evaluating the impact of assimilating HF-Radar observations and/or Waverider buoy data on model forecast skill. A significant improvement in forecast skill beyond the current AUSWAVE system could justify the significant expense of upgrading the SAG installation communications to provide near real time data streams to the Bureau.

Acknowledgments

HF-Radar Data was sourced from the Integrated Marine Observing System (IMOS) - IMOS is a national collaborative research infrastructure, supported by the Australian Government. The Cape du Couedic Waverider Buoy Data was supplied by the Australian Bureau of Meteorology. The ADCP wave data was supplied by the SARDI Innovative Solutions 2 (IS2) project. The grid for the wave model was the SAROM grid from the eSA-Marine forecasting system run by SARDI and the Australian Bureau of Meteorology.

References

ACCESS-R: Australian Bureau of Meteorology regional weather model.

BRAN 2015, Bluelink Re-Analysis (global re-analysis of OFAM) April 2009-July 2015

Booij, N., R. C. Ris, and L. H. Holthuijsen, 1999, A third-generation wave model for coastal regions, 1, Model description and validation, J. Geophys. Res., 104, C4, 7649-7666.

Cosoli, S., B. Grcic, S. De Vos, and Y. Hetzel, 2018. Improving data quality for the Australian High Frequency Ocean radar network through Real-Time and Delayed-Mode quality-control procedures. Remote Sensing 10, 1476.

Dee, D. P., Uppala, S. M., Simmons, A. J., Berrisford, P., Poli, P., Kobayashi, S., Andrae, U., Balmaseda, M. A., Balsamo, G., Bauer, P., Bechtold, P., Beljaars, A. C. M., van de Berg, L., Bidlot, J., Bormann, N., Delsol, C., Dragani, R., Fuentes, M., Geer, A. J., Haimberger, L., Healy, S. B., Hersbach, H., Hólm, E. V., Isaksen, L., Kållberg, P., Köhler, M., Matricardi, M., McNally, A. P., Monge-Sanz, B. M., Morcrette, J.-J., Park, B.-K., Peubey, C., de Rosnay, P., Tavolato, C., Thépaut, J.-N. and Vitart, F., 2011, The ERA-Interim reanalysis: configuration and performance of the data assimilation system, Q. J. R. Meteorol. Soc., 137: 553–597

Egbert, G.D., and S.Y. Erofeeva, 2002, Efficient inverse modeling of barotropic ocean tides, J. Atmos. Oceanic Technol., 19(2), 183-204.)

Fisher, N. I., 1995, Statistical Analysis of Circular Data, Cambridge University Press.

Gomez, R., L. R. Wyatt, L. Guiomar, N. Thomas, S. Smet, and Guillaume Sicot, 2015, Estimation of wave parameters from HF radar using different methodologies and compared with wave buoy measurements at the Wave Hub. OCEANS 2015 - Genova, Genoa, 2015, 1-9.

Green, J. J., and L. R. Wyatt, 2006, Row-action inversion of the Barrick-Weber equations. J. Atmos. Oceanic Technol., 23, 501-510.

Greenslade, D. J. M., and I. R. Young. 2005, The impact of altimeter sampling patterns on estimates of background errors in a global wave model. Journal of Atmospheric and Oceanic Technology 22.12, 1895-1917.

Groen, P., and R. Dorrestein, 1976, Zeegolven. KNMI Opstellen op oceanografisch en maritiem meteorologisch gebied. Dutch. State Printing Office, The Hague.

Gurgel, K. -W., G. Atnonischki, H. Essen, H. H., and T. Schlick, 1999. Wellen Radar (WERA): a new ground-wave HF radar for ocean remote sensing. Coastal Engineering 37, 219-234.

Haidvogel, Dale B., H. G. Arango, K. Hedstrom, A. Beckmann, P. Malanotte-Rizzoli, and Al. F. Shchepetkin, 2000, Model evaluation experiments in the North Atlantic Basin: simulations in nonlinear terrain-following coordinates. Dynamics of atmospheres and oceans 32.3, 239-281.

Hemer, M. A., J. A. Church, and J. R. Hunter, 2010, Variability and trends in the directional wave climate of the Southern Hemisphere. International Journal of Climatology 30.4, 475-491.

Heron, M. L., A. Prytz, 2002, Wave height and wind direction from the HF coastal ocean surface radar, Canadian J. Remote Sensing, 28, 385-393.

Hisaki, Y., 2014, Intercomparison of wave data obtained from single high-frequency radar, in situ observations and model prediction. Int. J. Remote Sensing, 35 (10), 26pp

IMOS 2017, South Australia Gulfs HF radar (SA) - Real-time sea water velocity, accessed 2011-2014.

Long, R. M., D. Barrick, J. L. Largier, and N. Garfield, 2011, Wave observations from Central California: SeaSonde Systems and in situ wave measurements. J. of Sensors, 2011, 18pp.

Lorente, P., M.G. Sotillo, L. Aouf, A. Amo-Baladrón, E. Barrera, A. Dalphinet, C. Toledano, R. Rainaud, M. De Alfonso, S. Piedracoba, A. Basañez, J. M. García-Valdecasas, V. Pérez- Muñuzuri, and E. Álvarez-Fanjul, 2018, Extreme Wave Height Events in NW Spain: A Combined Multi-Sensor and Model Approach. Remote Sensing, 10, 1.

Middleton, J. F., M. Doubell, C. James, J. Luick, P. van Ruth, 2013, PIRSA Initiative II: carrying capacity of Spencer Gulf: hydrodynamic and biogeochemical measurement modelling and performance monitoring. SARDI Publication No. F2013/000311-1. SARDI Research Report Series No. 705. 96pp.

WMO, Secretariat. 1998, Guide to Wave Analysis and Forecasting.

Wyatt L.R, 2012, Shortwave direction and spreading measured with HF radar, Journal of Atmospheric and Oceanic Technology, 29, 286-299.

Waters, J., L. R. Wyatt, J. Wolf, and A. Hines, 2013, Data assimilation of partitioned HF radar wave data into Wavewatch III, Ocean Modelling, 72, 17-31.

Wyatt, L. R., J. J. Green, and A. Middleditch, 2011, HF radar data quality requirements for wave measurement. Coastal Eng., 58, 327-336.

Wyatt, L. R., J. J. Green, and A. Middleditch, 2009, Signal sampling impacts on HF radar wave measurement. J. Atmos. Oceanic Technol., 26, 793-805.

Wyatt, L. R., J. J. Green, A. Middleditch, M. D. Moorhead, J. Howarth, M. Holt, and S. Keogh, 2006, Operational wave, current and wind measurements with the Pisces HF radar. IEEE J. Oceanic. Eng., 31, 819-834.

Wyatt, L. R., J. J. Green, K.-W. Gurgel, J.C. Nieto Borge, K. Reichert, K. Hessner, H. Gunther, W. Rosenthal, O. Saetra, and M. Reistad, 2003, Validation and intercomparisons of wave measurements and models during the EuroROSE experiments. Coastal Engineering, Vol 48, 1-28.

Wyatt, L. R., S.P. Thompson, and R. R. Burton, 1999, Evaluation of high frequency radar wave measurement. Coastal Engineering, Vol. 37, 259-282.

Figure Captions

Figure 1: Map of South Australian Shelf showing location of HF-Radar installation, the SAROM model domain, and sources of data.

Figure 2: Comparison between Wave Observations and SWAN Model in Spencer Gulf at Cape du Couedic (top panel) and the IS2 ADCP mooring (bottom panel).

Figure 3: Comparison of HF-Radar wave observations (green points) of significant wave height with Waverider measurements at Cape du Couedic (black) and results of the SWAN simulation (red) at the HF-Radar site for the three observational periods.

Figure 4: Comparison of HF-Radar wave observations (green points) of peak wave period with Waverider measurements at Cape du Couedic (black) and results of the SWAN simulation (red) at the HF-Radar site for the three observational periods.

Figure 5: Comparison of HF-Radar wave observations (green points) of peak wave direction with the results of the SWAN simulation (red) at the HF-Radar site for the three observational periods.

Figure 6: Comparison of HF-Radar wind observations (green points) of direction with in-situ measurements from Neptune Island (blue) for the three observational periods.

Figure 7: Comparison of significant wave height measured by HF-Radar and Waverider buoy: correlation and statistics (top panel) and coherence squared and phase (bottom).

Figure 8: Comparison of peak wave period measured by HF-Radar and Waverider buoy: correlation and statistics (top panel) and coherence squared and phase (bottom).

Figure 9: Comparison of significant wave height from coupled SWAN-ROM model at HF-Radar and Waverider buoy sites: correlation and statistics (top panel) and coherence squared and phase (bottom).

Figure 10: Comparison of Wind direction measured by HF-Radar significant and Neptune Island AWS: circular correlation and statistics (top panel) and coherence squared and phase (bottom).

Table Caption

Table 1: Summary of statistics for all inter-comparisons of time series shown in this paper. The comparison time series are: SWAN model output (Model), ADCP (IS2), Waverider buoy (CdC), and HF Radar. The figure where the time series and/or statistics are displayed are listed under Reference figure. The variables are: significant wave height (Hs), peak wave period (Tp), peak wave direction (Pdir), and wind direction (Wdir). Note that the means and standard deviations are calculated for the times where the time series overlap so that there will be differences for the same variable when compared to different time series. Highlighted cases are subject to coherence analysis in the text.

Table

Table 1: Summary of statistics for all inter-comparisons of time series shown in this paper. The comparison time series are: SWAN model output (Model), ADCP (IS2), Waverider buoy (CdC), and HF Radar. The figure where the time series and/or statistics are displayed are listed under Reference figure. The variables are: significant wave height (Hs), peak wave period (Tp), peak wave direction (Pdir), and wind direction (Wdir). Note that the means and standard deviations are calculated for the times where the time series overlap so that there will be differences for the same variable when compared to different time series. Highlighted cases are subject to coherence analysis in the text.

								V
Comparison	Reference Figure	Variables	Num. of Obs.	Corr.	RMSE	NRMSE	Bias	Mean
Model vs IS2	Figure 2 top	Hs (m)	671	0.80	0.44	28%	0.17	1.55
Model vs CdC	Figure 2 bottom	Hs (m)	5568	0.95	0.39	15%	0.15	2.64
HF Radar vs CdC	**Figures 3 and 7**	**Hs (m)**	**10311**	**0.90**	**0.42**	**15%**	**0.06**	**2.87**
Model vs CdC	Figure 3	Hs (m)	49523	0.93	0.44	15%	-0.18	2.86
HF Radar vs Model	Figure 3	Hs (m)	10209	0.87	0.52	18%	0.20	2.87
HF Radar vs CdC	**Figures 4 and 8**	**Tp (sec)**	**14302**	**0.80**	**1.31**	**10%**	**0.32**	**12.81**
Model vs CdC	Figure 4	Tp (sec)	49524	0.70	1.47	11%	-0.23	12.96
HF Radar vs Model	Figure 4	Tp (sec)	14053	0.67	1.55	12%	0.43	12.82
HF Radar vs Model	Figure 5	Pdir (deg.)	14500	0.02	32.01	9%	-0.54	-138.
Model vs Model	**Figure 9**	**Hs (m)**	**13433**	**0.99**	**0.15**	**5%**	**-0.08**	**2.84**
HF Radar vs AWS	**Figures 6 and 10**	**Wdir (deg.)**	**29734**	**0.87**	**26.38**	**7%**	**-3.59**	**-174.**

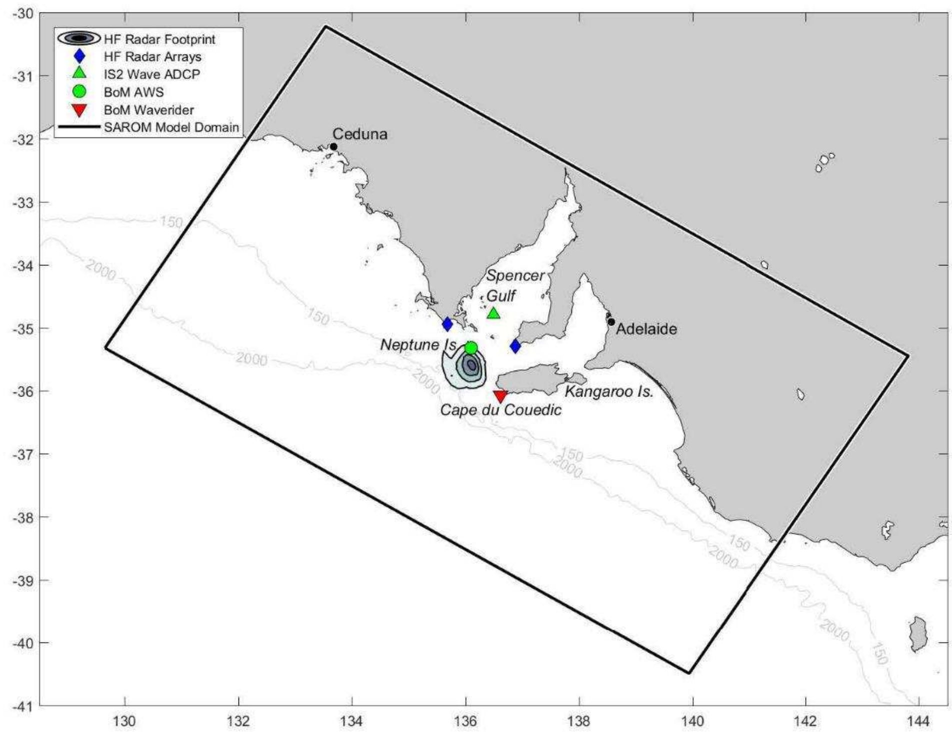

Figure 1: Map of South Australian Shelf showing location of HF-Radar installation, the SAROM model domain, and sources of data.

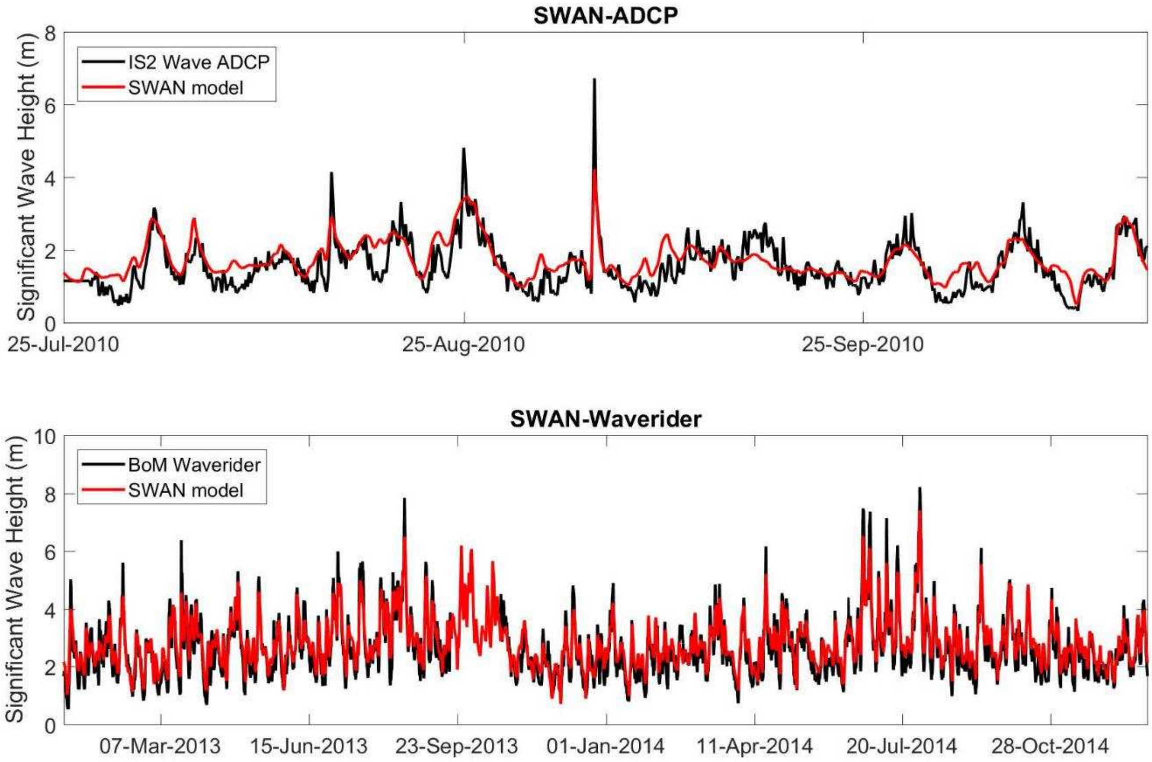

Figure 2: Comparison between Wave Observations and SWAN Model in Spencer Gulf at Cape du Couedic (top panel) and the IS2 ADCP mooring (bottom panel).

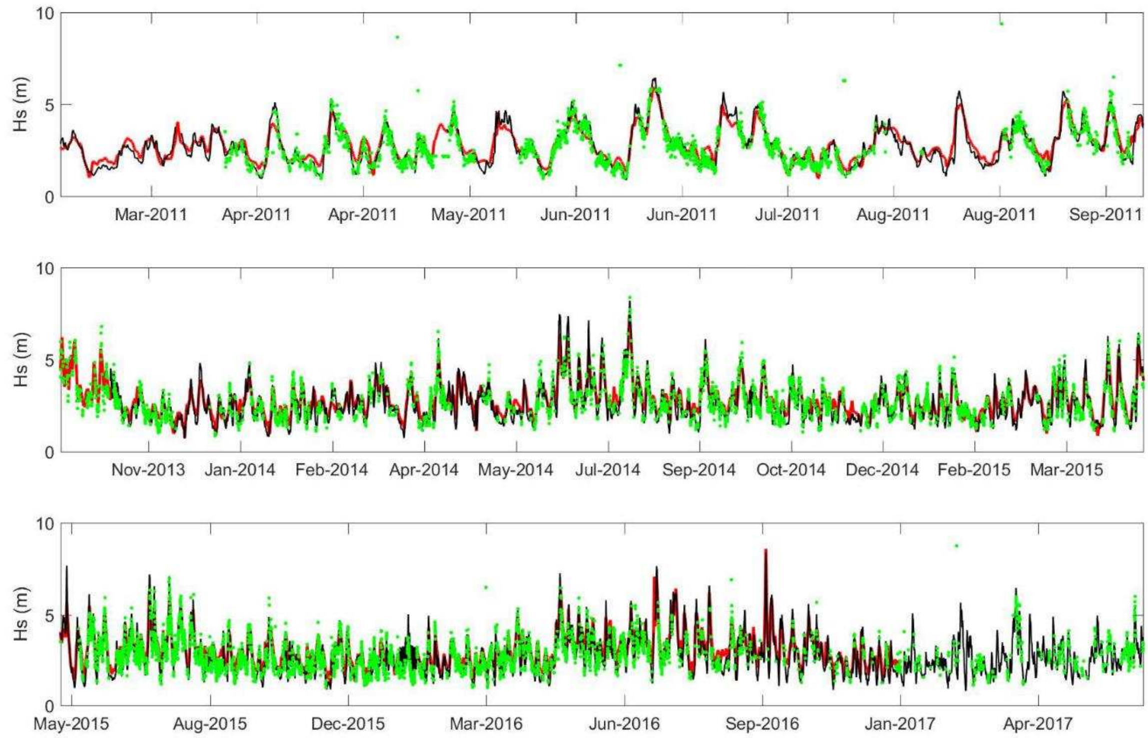

Figure 3: Comparison of HF-Radar wave observations (green points) of significant wave height with Waverider measurements at Cape du Couedic (black) and results of the SWAN simulation (red) at the HF-Radar site for the three observational periods.

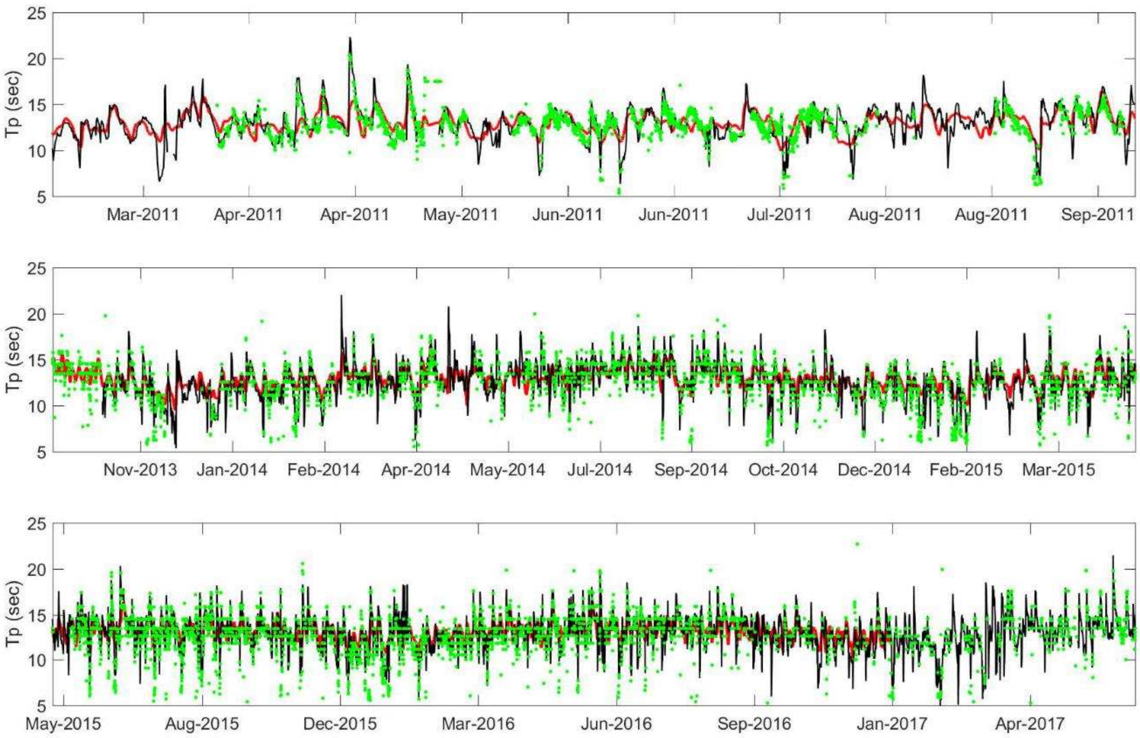

Figure 4: Comparison of HF-Radar wave observations (green points) of peak wave period with Waverider measurements at Cape du Couedic (black) and results of the SWAN simulation (red) at the HF-Radar site for the three observational periods.

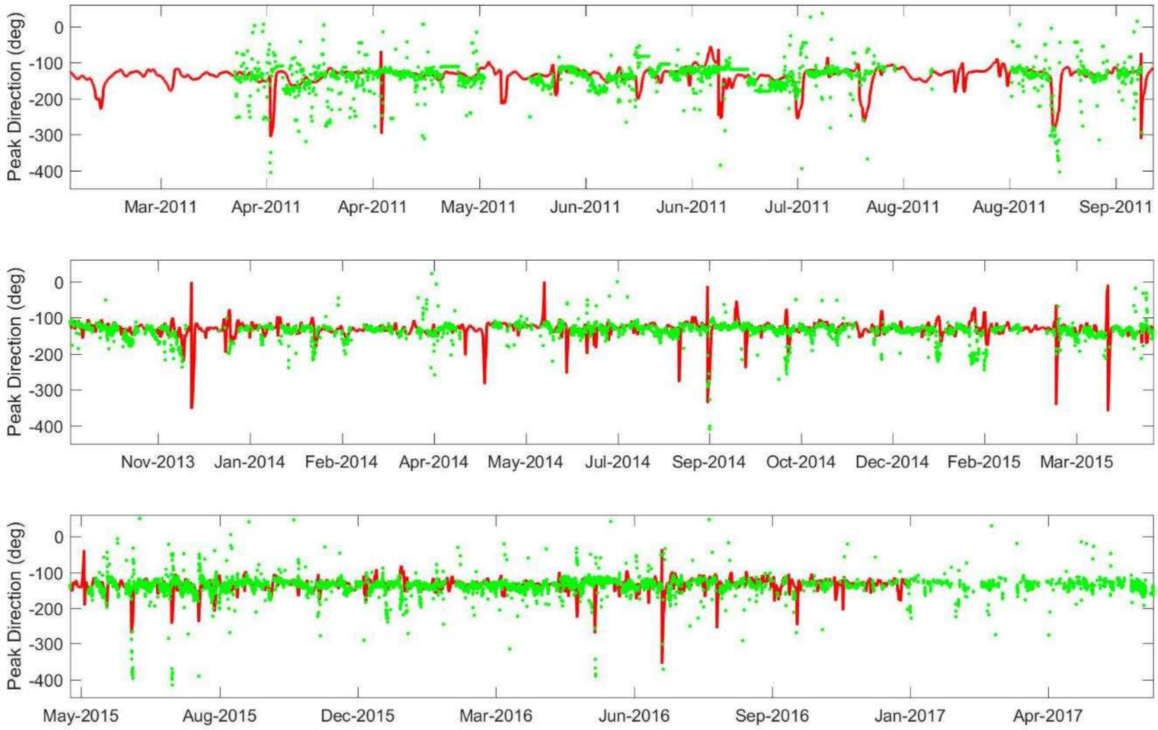

Figure 5: Comparison of HF-Radar wave observations (green points) of peak wave direction with the results of the SWAN simulation (red) at the HF-Radar site for the three observational periods.

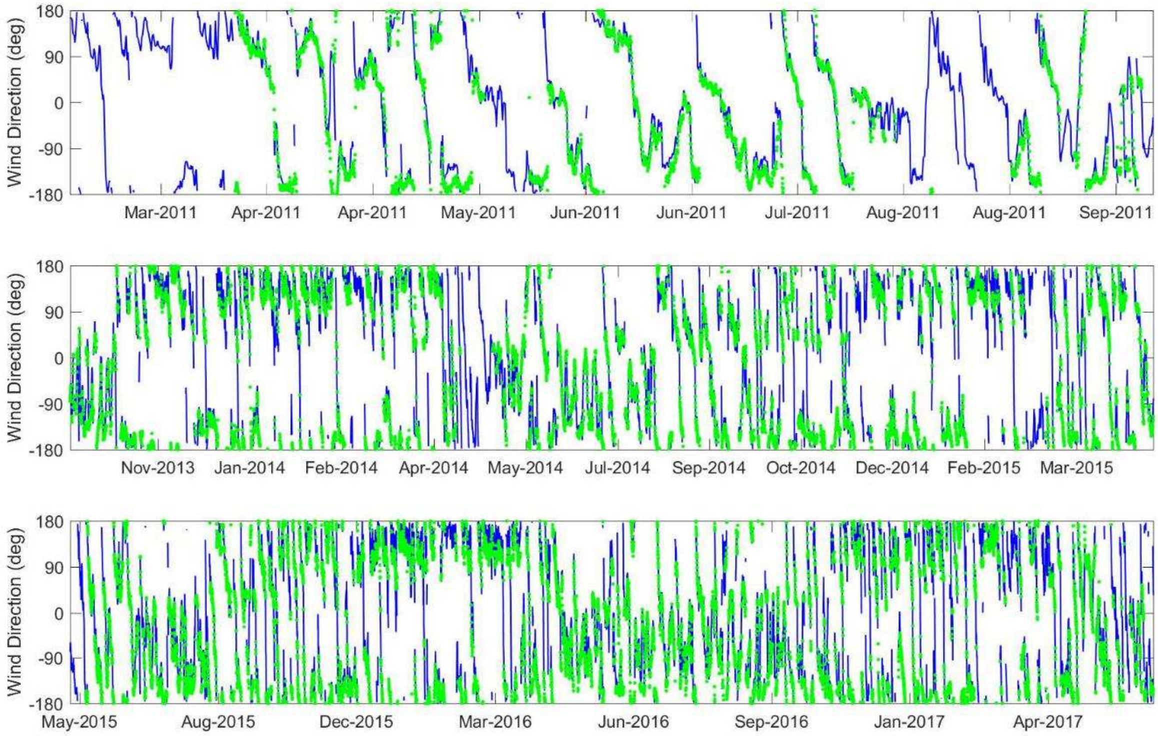

Figure 6: Comparison of HF-Radar wind observations (green points) of direction with in-situ measurements from Neptune Island (blue) for the three observational periods.

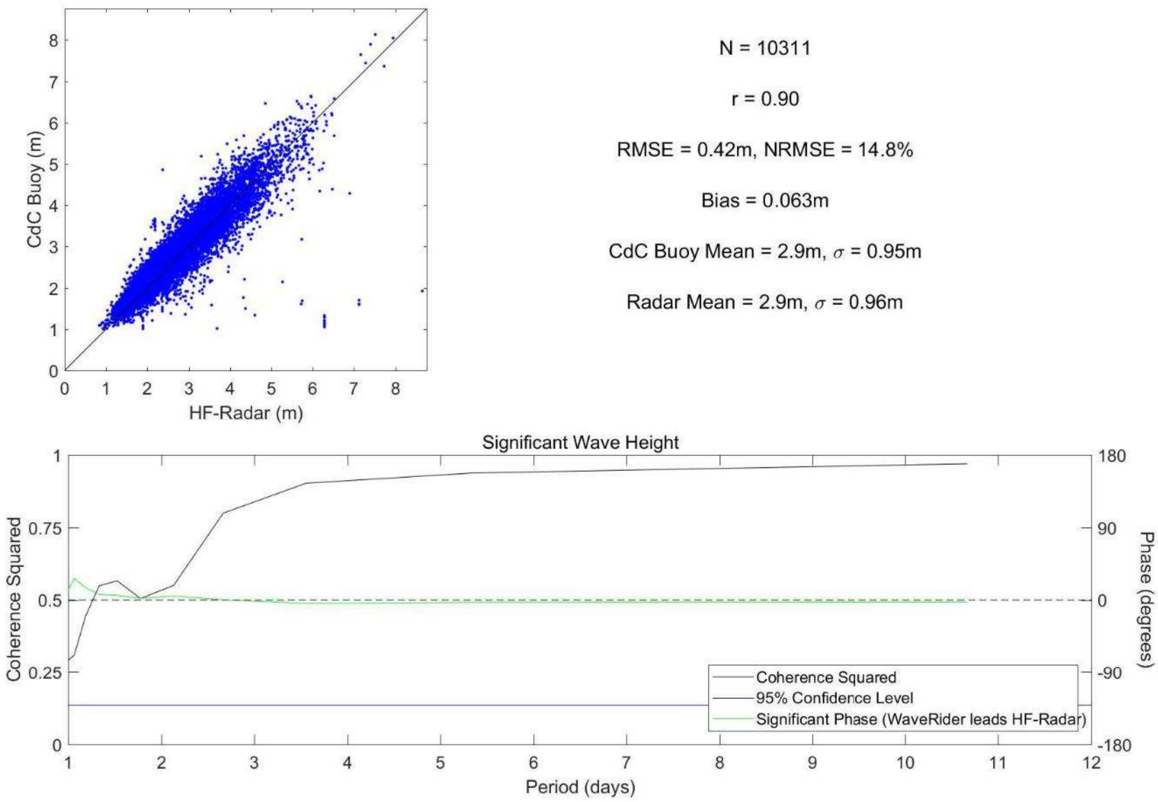

Figure 7: Comparison of significant wave height measured by HF-Radar and Waverider buoy: correlation and statistics (top panel) and coherence squared and phase (bottom).

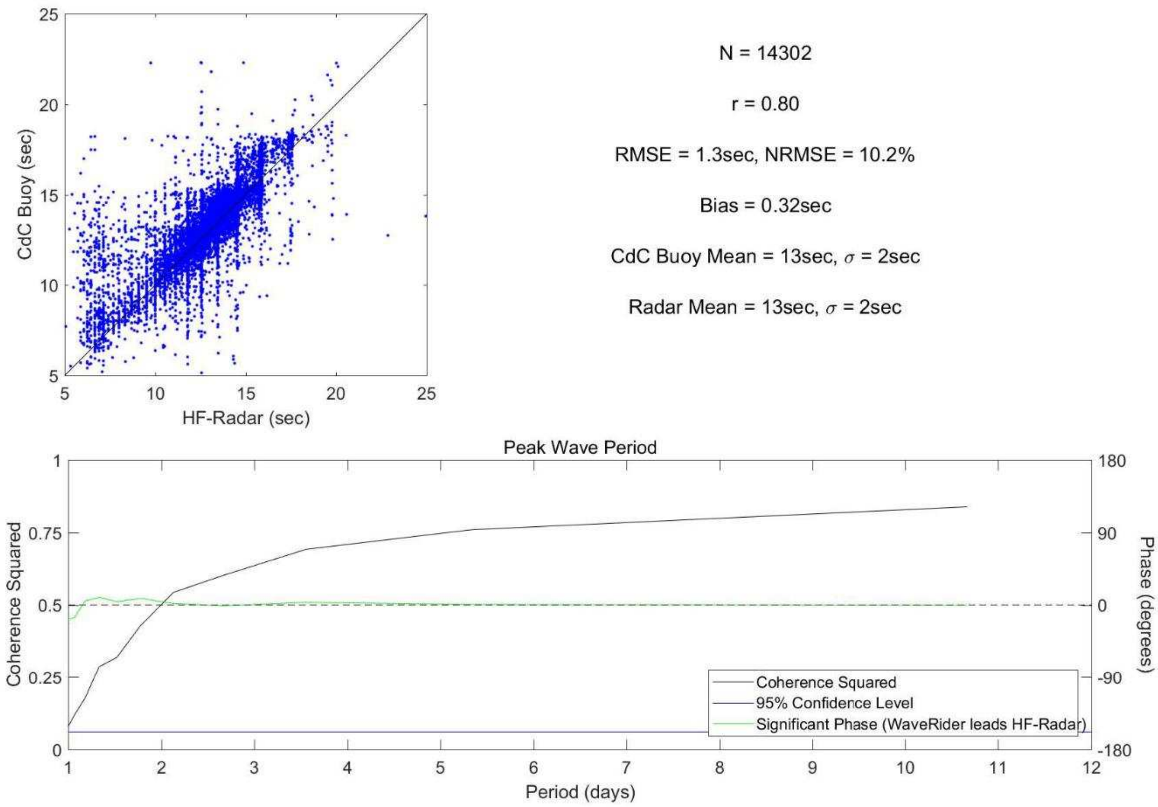

Figure 8: Comparison of peak wave period measured by HF-Radar and Waverider buoy: correlation and statistics (top panel) and coherence squared and phase (bottom).

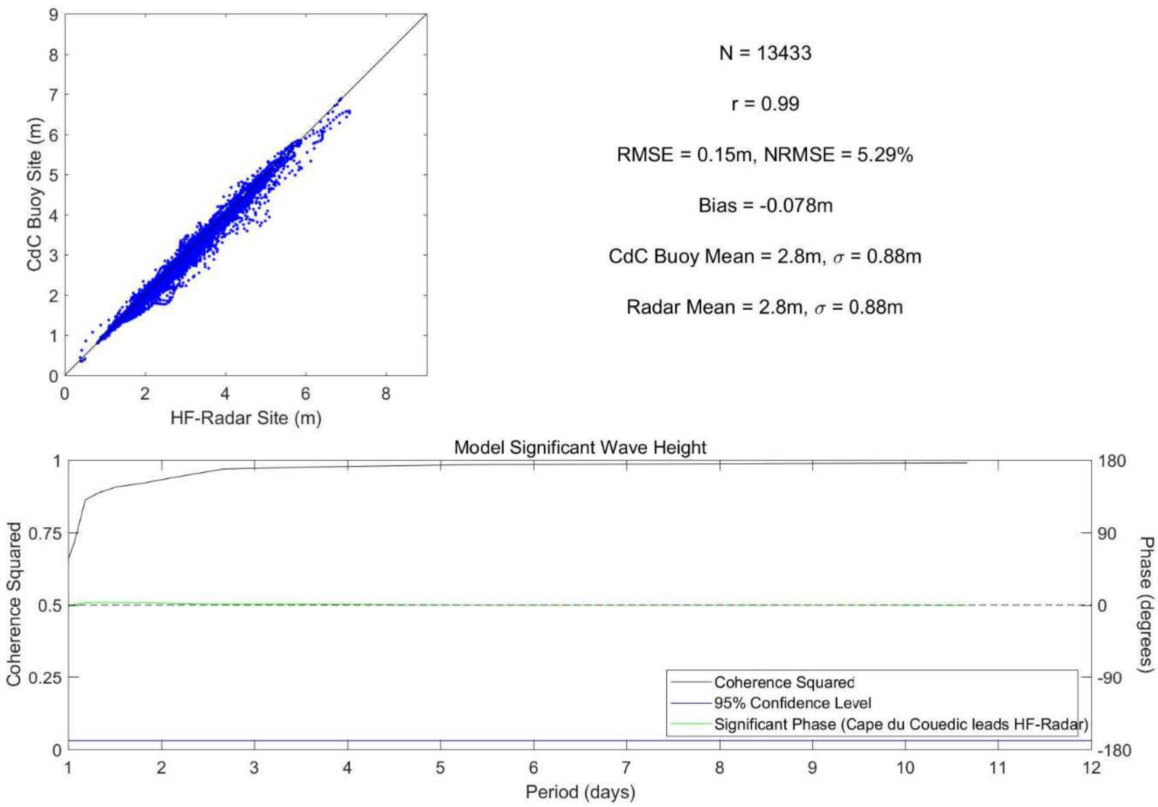

Figure 9: Comparison of significant wave height from coupled SWAN-ROM model at HF-Radar and Waverider buoy sites: correlation and statistics (top panel) and coherence squared and phase (bottom).

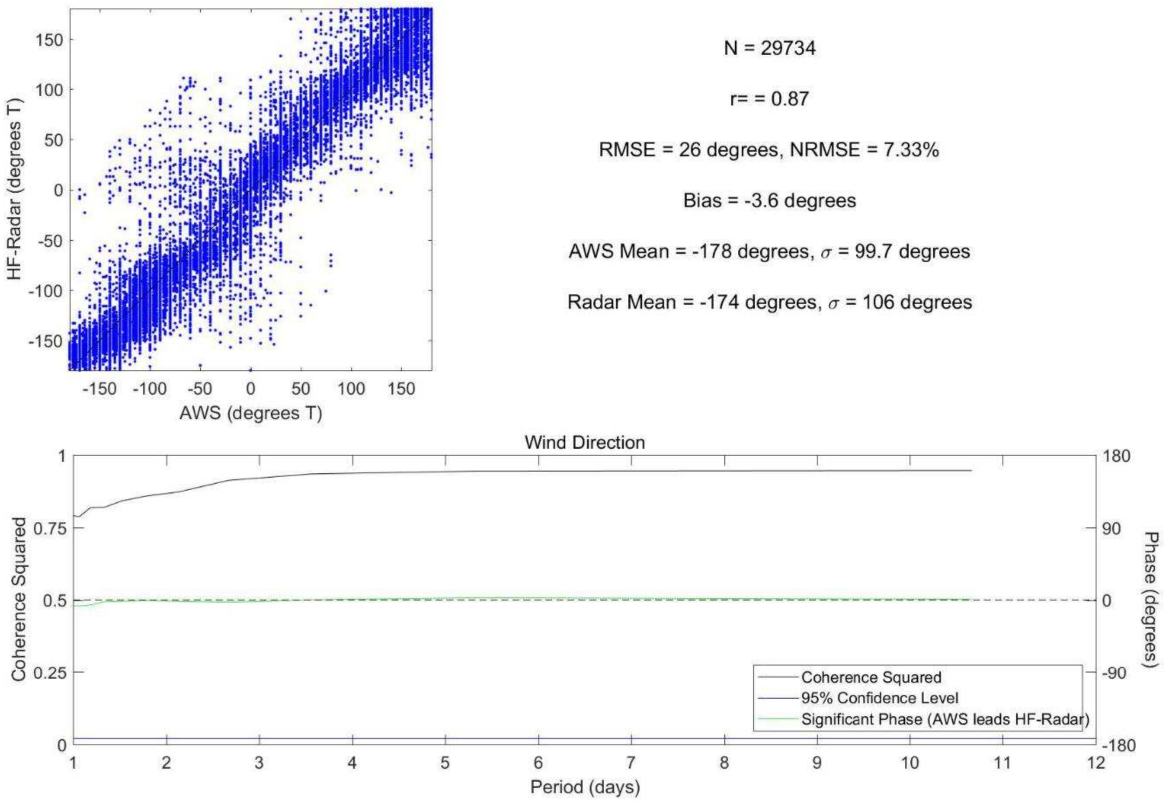

Figure 10: Comparison of Wind direction measured by HF-Radar significant and Neptune Island AWS: circular correlation and statistics (top panel) and coherence squared and phase (bottom).